

# Classical Half-Adder using Trapped-ion Quantum Bits: Towards Energy-efficient Computation

Sagar Silva Pratapsi,<sup>1,2</sup> Patrick H. Huber,<sup>3</sup> Patrick Barthel,<sup>3</sup>  
Sougato Bose,<sup>4,5</sup> Christof Wunderlich,<sup>3</sup> and Yasser Omar<sup>1,6,7</sup>

<sup>1</sup>*Instituto Superior Técnico, Universidade de Lisboa, Portugal*

<sup>2</sup>*Instituto de Telecomunicações, Portugal*

<sup>3</sup>*Department of Physics, School of Science and Technology, University of Siegen, 57068 Siegen, Germany*

<sup>4</sup>*Department of Physics and Astronomy, University College London, London WC1E 6BT, UK*

<sup>5</sup>*Department of Electronic & Electrical Engineering,  
University College London, WC1E 7JE London, UK*

<sup>6</sup>*Physics of Information and Quantum Technologies Group,  
Centro de Física e Engenharia de Materiais Avançados (CeFEMA), Portugal*

<sup>7</sup>*PQI – Portuguese Quantum Institute, Portugal*

(Dated: October 20, 2022)

We propose, and realise experimentally, Toffoli and Half-Adder circuits suitable for classical computation, using radiofrequency-controlled  $^{171}\text{Yb}^+$  ions in a macroscopic linear Paul-trap as qubits. We analyse comprehensively the energy required to operate the logic gates, both theoretically and experimentally. We identify bottlenecks and possible improvements in future platforms for energetically-efficient computation, *e.g.*, trap chips with integrated antennas and cavity QED. Based on our analysis, a novel planar ion trap is expected to be  $10^5$  times more efficient. Our experimentally verified energetic model fills a gap in the literature of the energetics of quantum information, and outlines the path for its detailed study, as well as its potential applications to classical computing.

*Introduction.*— Computational tasks are responsible for a non-negligible part of the world’s energy consumption. It is estimated that computationally-intensive data-centres represent 1% of the global energy budget [1]. So far, increases in energy efficiency have been able to offset the growing demand for computation: peak-usage energy efficiency has doubled every 1.5 years during the 1960–2000 period, while since the 2000s this figure is closer to 2.6 years [1, 2].

However, processor efficiency gains cannot continue to grow forever. There is a fundamental limitation of the current paradigm of non-reversible computation, known as Landauer’s principle [3], where each irreversible bit operation dissipates  $k_B T \ln 2$  of heat.

Reversible computation may thus become an important computation paradigm in the future. Reversible systems may also avoid the heat costs of contemporary CMOS processors, such as capacitor charging, switching and current leakage [4, 5], which are ultimately responsible for the typical 40% energy cost for cooling in data centres [6]; they may also protect against external attacks such as power usage analysis. It is, then, worthwhile to investigate how energy-efficient reversible platforms can become.

Some proposals for reversible computing platforms have been billiard-ball models [7, 8], adiabatic circuits [9–13], nano-machines [14–18], superconducting devices [19–21], quantum-dot cellular automata [22], and others (see [23] for a review of reversible computation).

Quantum mechanical systems, which evolve unitarily, are also reversible by nature, and are thus an attractive candidate for energetically efficient computation [24, 25]. Although quantum platforms are limited by coherence time, we can reset the coherence for classical computations by measuring in the computational basis in-between logical operations. We may also ex-

exploit super-selection rules to protect classical information, as was proposed recently in a quantum dot platform [26]. Can we then build energy efficient circuits for universal reversible computation using quantum computing platforms?

In this work, we propose, and experimentally realise, a trapped-ion classical Half-Adder circuit, an important building block for arithmetic operations in computer processors [27]. To do so, we implement a Toffoli gate, itself a universal gate for classical computation. We determine the energy to operate these gates, both theoretically and experimentally, and point out possible improvements towards energy efficient computation.

Some works, such as [28], require realistic estimates for the energy consumed by quantum computers. Thus, our energetic analysis, supported by experimental measurements, also fills a gap in the literature, and is a first step towards understanding the energetic impact of quantum technologies [29].

*Gate proposals.*— A Half-Adder circuit is a fundamental component of arithmetic circuits. It computes the logical AND (multiplication modulo 2) and XOR (addition modulo 2) of two input bits. It is a building block for the Full-Adder circuit, addition circuits in their ripple-carry and carry-lookahead variants, multiplier circuits and other tasks in contemporary computer processors. The core operation behind our Half-Adder circuit is a quantum Toffoli gate, followed by the application of a CNOT to the two control qubits of the Toffoli (FIG. 1).

A Toffoli gate, or a controlled-controlled-NOT gate, is a universal three-bit operation, *i.e.*, it is sufficient to construct any classical reversible circuit. Antonio *et al.* proposed a Toffoli gate suitable for classical computation [30], which can be realised on any three-qubit physical system with constant nearest-neighbour Ising

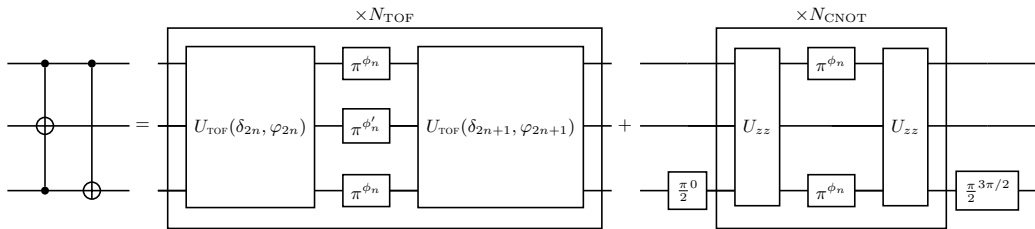


FIG. 1. **A Half-adder circuit** using a Toffoli followed by a CNOT gate. We choose the central qubit as the target of the Toffoli gate to fulfill the condition  $J_{12} = J_{23}$  from Equation (1). **The Toffoli gate** decomposes into a unitary  $U_{\text{TOF}}(\delta_n, \phi_n)$  (generated from Hamiltonian (3) for 14.9 ms/400) and single qubit  $\pi$ -pulses with some phase  $\phi$  ( $\pi^\phi$ , implementing Dynamical Decoupling). The block is repeated  $N_{\text{TOF}} = 200$  times with updated values of  $\delta_n$ ,  $\varphi_n$  and DD phases  $\phi_n$  and  $\phi'_n$ . The latter are chosen to implement a universal robust DD sequence on qubits 1 and 3 and a CPMG<sub>XY</sub> on qubit 2. The values  $(\delta_{2n}, \delta_{2n+1})$  alternate between  $(\delta, -\delta)$  and  $(-\delta, \delta)$  for each  $\pi$ -pulse, while  $(\varphi_{2n}, \varphi_{2n+1})$  alternates between  $(0, \pi)$  and  $(\pi, 0)$  for each  $\pi^{\pi/2}$ -pulse. **The CNOT gate** decomposes into a  $U_{zz}$  gate (implementing the  $zz$  coupling) and single qubit  $\pi$ -pulses. The block is repeated  $N_{\text{CNROT}} = 120$  times. The phases  $\phi_n$  implement a UR DD sequence on the control and target qubits.

couplings, via the Hamiltonian

$$H_{\text{TOF}} = \frac{\hbar J}{2} (\sigma_1^z \sigma_2^z + \sigma_2^z \sigma_3^z) + \frac{\hbar \delta}{2} \sigma_2^z + \frac{\hbar \Omega}{2} \sigma_2^x. \quad (1)$$

Here,  $\sigma_j^i$  is the  $\sigma^i$  Pauli operator acting on the  $j$ -th qubit, appropriately tensored with the identity operators on the other qubits. The real constants  $J$ ,  $\delta$  and  $\Omega$  define interaction strengths. We simulated numerically the time evolution under the Hamiltonian (1) for a time of  $\pi/\Omega$  and  $\delta = 2J$ . We found that  $\Omega \approx 1.1J$  allows for a  $\approx 99\%$  classical Toffoli gate fidelity while minimising the gate time (see Supplemental Material).

*Experimental implementation.*— Ions confined in a linear Paul trap are natural candidates to implement the Hamiltonian (1) [30, 31]. We use  $^{171}\text{Yb}^+$  ions confined in a linear Paul trap, with a superimposed static magnetic field gradient [32]. The qubit states  $|0\rangle$  and  $|1\rangle$  are the two hyperfine states of the electronic ground state  $^2S_{1/2}$  with total angular momentum quantum number and magnetic quantum number  $|F, m_F\rangle = |0, 0\rangle$  and  $|1, 1\rangle$ , connected by a magnetic dipole resonance near  $2\pi \times 12.6$  GHz. The  $|1\rangle$  state is sensitive to the magnetic field, which is position dependent, shifting individually the ions' resonances and, thus, allowing for individual addressing by tuning the microwave field driving the qubit resonance [33].

When irradiating the ions with a microwave field with phase  $\phi$  and frequency  $\omega_x$ , nearly resonant with the frequency  $\omega_2$  of qubit 2, the ionic qubits are subject to the Hamiltonian

$$H^{(i)} = \underbrace{\sum_{i \neq j} \frac{\hbar J_{ij}}{2} \sigma_i^z \sigma_j^z}_{H_{zz}} + \sum_j \frac{\hbar \omega_j \sigma_j^z}{2} + \hbar \Omega \cos(\omega_x t + \phi) \sigma_2^x. \quad (2)$$

Here,  $\omega_i$  is the resonance frequency of the  $i^{\text{th}}$  ion. The two-qubit couplings  $J_{ij}$  in a magnetic field gradient are mediated by the Coulomb interaction [31, 32]. In the setup used here, the magnetic field gradient is 19.1 T/m at a secular axial trap frequency of  $\omega_T = 2\pi \times 128.4(1)$  kHz, and  $J_{12} = J_{23} = J \approx 2\pi \times 31$  Hz,

which implies a gate time of  $\pi/1.1J \approx 14.9$  ms. The additional  $J_{13} \sigma_1^z \sigma_3^z$  coupling contributes with a complex phase in the computational basis, which is irrelevant for classical computation, so we choose to omit it. Finally,  $\Omega$  is determined by the amplitude of the incident microwave radiation.  $H_{zz}$  is the Hamiltonian generating the required spin-spin interaction via magnetic gradient induced coupling (MAGIC). Cross-talk between qubits was neglected; its main source is the non-resonant excitation of neighbouring qubits which has been measured to be on the order  $10^{-5}$  [33].

Choosing a detuning  $\delta$ , such that  $\omega_x = \omega_2 - \delta$ , and in an appropriate rotating frame,  $H_I$  reads as

$$H_I^{(i)} \approx H_{zz} + \frac{\hbar \delta}{2} \sigma_2^z + \frac{\hbar \Omega}{2} (\cos(\phi) \sigma_2^x + \sin(\phi) \sigma_2^y), \quad (3)$$

with an error of  $O(\Omega/(2\omega_2 - 2\delta))$  [30]. Choosing  $\phi = 0$  recovers the Hamiltonian (1).

*Dynamical Decoupling (DD).* Fluctuations in the magnetic field dephase the qubits, which are first-order sensitive to them. Not using passive magnetic shielding and active compensation, the coherence time in this setup is  $\approx 200 \mu\text{s}$  [34] – two orders of magnitude lower than our gate times. We thus employ Dynamical Decoupling (DD) to protect the qubits.

For DD we intersperse single-qubit  $\pi$  rotations in-between the Hamiltonian evolution, by periodically irradiating the qubits with a top hat-shaped pulse of Rabi frequency  $2\pi \times 33$  kHz. The  $J_{ij}$  couplings are negligible during this time, since they are three orders of magnitude smaller than the Rabi frequency. We use the notation  $\theta^\phi$  for a Rabi rotation of angle  $\theta$  with phase  $\phi$ :  $\pi^0$  and  $\pi^{\pi/2}$  are thus  $\sigma^x$  and  $\sigma^y$  gates, respectively (see Eq. (3)).

Applying a  $\pi$ -pulse amounts to a change of basis, so we need to change the Hamiltonian evolution accordingly. The  $\sigma_2^z$  term acquires a relative minus sign, since  $\sigma_i^z \sigma_i^{x,y} = -\sigma_i^{x,y} \sigma_i^z$ , which we compensate by changing the microwave detuning as  $\delta \rightarrow -\delta$ . On the other hand, the  $\sigma_i^z \sigma_j^z$  terms are left unchanged when both qubits are flipped simultaneously. The  $\sigma_2^x$  term acquires a minus sign when a  $\sigma_2^y$  pulse is applied, which we compensate by adding a phase of  $\phi = \pi$  to

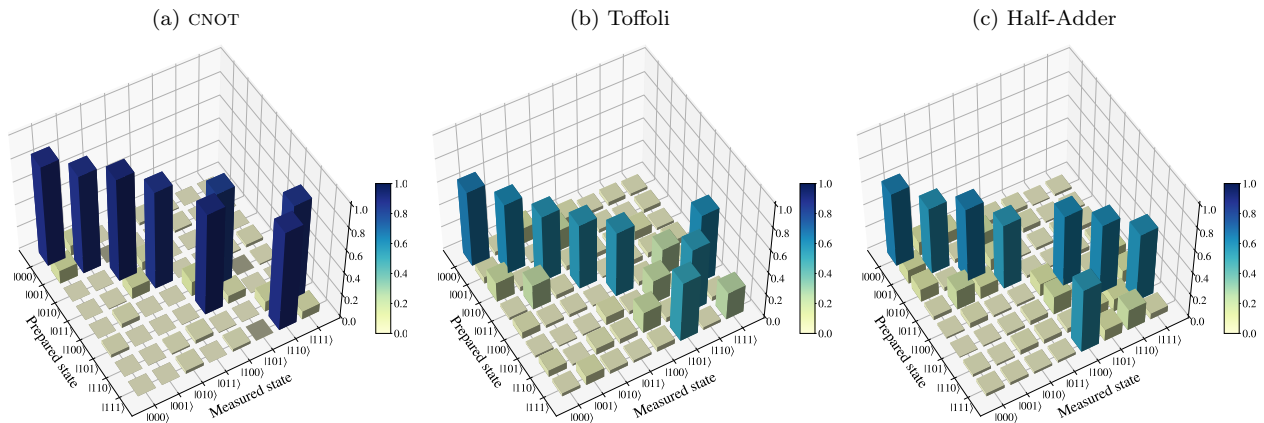


FIG. 2. Measurement probabilities for the CNOT, Toffoli and Half-Adder gates, reconstructed from Maximum-Likelihood Estimate tomography. The CNOT gate is controlled by qubit 1 and acts on qubit 3, while the Toffoli gate has qubit 2 as a target. The CNOT, Toffoli and Half-adder gates have classical fidelities of 86.9%, 58.8% and 60.6%, respectively.

the driving field's phase. This limits the applicable DD-sequences to either  $\sigma^x$  or  $\sigma^y$  pulses.

For the Toffoli gate, we choose the Carr-Purcell-Meiboom-Gill pulse sequence [34, 35] CPMG<sub>XY</sub> applied to the target qubit and a Universal Robust (UR) sequence [36] applied to the control qubits (see FIG. 1).

*CNOT gate.* The CNOT gate implementation using the MAGIC scheme is realised by a  $(\pi/2)^0$ -pulse on the target qubit, and a unitary evolution generated by  $H_{zz}$  inducing a relative phase change of  $\pi$  conditioned on the logical state of the control qubit. Finally, a  $(\pi/2)^{3\pi/2}$ -pulse is applied to the target [32]. In a register exceeding size 2, it is necessary to decouple the spectator qubits from the qubits carrying out the CNOT [32]. This is achieved using a DD-sequence on the qubits participating in the CNOT gate and excluding spectator qubits [34]. The conditional evolution time used in this work is  $T_{\text{CNOT}} \approx 8.75$  ms. We applied a UR sequence of 120 DD pulses, with a pulse duration of 15  $\mu$ s each to protect the qubits coherence [37]. The circuit diagram is shown in FIG. 1.

*Gate realisations.*— We implemented the CNOT, Toffoli and Half-Adder gates with classical fidelities of 86.9%, 58.8% and 60.6%, respectively (see Figure 2). The 90% Confidence Levels (CLs) are respectively [0.665, 0.937], [0.221, 0.683] and [0.409, 0.662], following the approach by Kiktento *et al.* [38]. The fidelities were calculated using Maximum-Likelihood process tomography [39]. The classical fidelity is the probability that the gate produces the correct output given a uniformly random computational state. We note that the CLs are overly conservative (see Figure 2 in [38] and related discussion). It is clear that the shorter CNOT time protects it against decoherence. A similar protection will be available for the Toffoli and Half-Adder in a next-generation trap, discussed at the end of this letter.

*Gate energetics.*— *Theoretical estimate.* Only Rabi oscillations are actively controlled, so the energy to perform the gates comes from the microwave pulses that drive the hyperfine transition  $|0\rangle \leftrightarrow |1\rangle$  via a magnetic dipole interaction.

The microwave pulses are generated by a cylindrical copper cavity coupled to a signal generator. The cavity diameter  $2a \equiv 16.3$  mm was chosen as to only allow the propagation of the dominant TE<sub>11</sub> mode, and to suppress higher-order modes. In the Supplemental Material we derive the power delivered by the cavity to achieve a qubit Rabi frequency of  $\Omega$ ,

$$P = \frac{1}{2} \frac{A_{\text{rad}}}{A_{\text{dip}}} \frac{\hbar\Omega^2}{\cos^2\theta}, \quad (4)$$

where  $A_{\text{rad}} \approx 1.9$  cm<sup>2</sup> and  $A_{\text{dip}} \approx 0.0034$  pm<sup>2</sup> can be respectively thought of as effective areas for the microwave pulse wavefront and the ions' magnetic dipole transition cross-section, and  $\theta$  is the angle between the ions' magnetic moments and the incident magnetic field. We take  $\cos\theta \approx 1$  to get a lower bound on the energy estimate.

In Table I, we summarise the energy estimates for all the implemented gates. The pulse energy is obtained by integrating the power in Equation (4) over the duration of each square pulse. The table also includes the number of  $\pi$ -pulses, or NOT gates, used in the DD scheme. The energy cost of a typical NOT gate in this implementation follows from Equation (4). For a Rabi frequency of  $2\pi \times 33$  kHz, we estimate a cost of 1.8  $\mu$ J.

*Measured power usage.* For a  $2\pi \times 33$  kHz Rabi frequency, a microwave signal requires 0.58 W in the current setup. This figure corresponds to the power delivered by the signal amplifier at the terminal of the vacuum recipient, measured with a spectrum analyser. Additional losses may occur during the transport of the signal to the antenna. The Toffoli was generated using a Rabi frequency of 34 Hz,  $10^3$  less than the Rabi frequency used to implement single qubit  $\pi$  and  $\pi/2$  rotations. Due to the low power, its cost was estimated assuming the law  $P \propto \Omega^2$  (see Equation (4)) as 9.2 nJ. In addition to the field generating the gate, there is the additional cost of the DD  $\pi$ -pulses. The power consumption of  $3 \times 200$   $\pi$ -pulses dominate the energetic costs of the Toffoli gate. These results are summarised in Table I.

| Gate       |           | MW Pulse    | Dyn. decoupling |         | Total       |
|------------|-----------|-------------|-----------------|---------|-------------|
|            |           |             | # $\pi$ -pulses | Cost    |             |
| NOT        | Estimated | 1.8 $\mu$ J | —               | —       | 1.8 $\mu$ J |
|            | Measured  | 8.8 $\mu$ J | —               | —       | 8.8 $\mu$ J |
| CNOT       | Estimated | 1.8 $\mu$ J | $2 \times 120$  | 0.44 mJ | 0.44 mJ     |
|            | Measured  | 8.8 $\mu$ J |                 | 2.1 mJ  | 2.1 mJ      |
| Toffoli    | Estimated | 2.0 nJ      | $3 \times 200$  | 1.1 mJ  | 1.1 mJ      |
|            | Measured  | 9.2 nJ      |                 | 5.3 mJ  | 5.3 mJ      |
| Half-Adder | Estimated | 1.8 $\mu$ J | 840             | 1.5 mJ  | 1.5 mJ      |
|            | Measured  | 8.8 $\mu$ J |                 | 7.4 mJ  | 7.4 mJ      |

TABLE I. Estimated and measured power consumption of the experimentally realised gates. “MW Pulse” refers to the microwave energy required to implement the Hamiltonian. “Total” includes the cost of dynamical decoupling  $\pi$ -pulses. For details, see Section *Measured Power Usage*.

Besides the pulse cost, there are other operational costs for carrying out computations which we divide into one-time costs and continuous costs. One-time costs include the energy dissipated for laser Doppler cooling, microwave-optical sideband cooling, and initial state preparation- and readout pulses. These tasks have to be carried out just once for a sequence of computational gates. They are achieved with a combination of two lasers, one near 369 nm and the other near 935 nm, and microwave pulses. Table II summarises the power consumed by these steps. The power figures were obtained by measuring the optical power of the laser beams, using a commercial optical power meter.

The most significant continuous cost is the power required to maintain the Paul trap, which is of the order of 10 W.

*Discussion and outlook.*— We implemented Toffoli and Half-Adder circuits which, together, open the door for new implementations of the logical operations present in contemporary processors, with the potential energy savings of reversible computation.

Based on our energetic analysis, we identify two energy bottlenecks. First, the microwave cavity produces a wavefront ( $A_{\text{rad}}$  in Eq. (4)) that is orders of magnitude larger than the ions’ interaction cross-section. For the NOT gate,  $\approx 10^{17}$  photons are irreversibly lost. Second, the conditional gate times are much longer than the qubits’ coherence times, making it necessary to use  $10^3$  DD pulses, where most of the energy is spent (see Table I).

A new planar ion trap setup [40] can address both of these issues. First, it integrates microwave antennae and resonators closer to the ions into a planar setup [41], which can greatly reduce the irreversible loss of microwave photons. For example, a NOT gate is performed in 0.4  $\mu$ s at an applied power of 10 mW, consuming 4 nJ of energy per gate, as opposed to 8.8  $\mu$ J.

In addition, the  $J$ -coupling, necessary for conditional gates, will be increased by about two orders of magnitude, thus reducing the time needed for CNOT, Toffoli and Half-Adder by the same factor. Further-

|                    | Laser 369 nm | Laser 935 nm | MW/ion | Duration | Energy       |
|--------------------|--------------|--------------|--------|----------|--------------|
| Doppler cooling    | 48.0 $\mu$ W | 1.35 mW      | 0.58 W | 8.0 ms   | 14 mJ        |
| Sideband cooling   | 0.16 $\mu$ W | 1.35 mW      | 0.58 W | 60 ms    | 100 mJ       |
| Ground state prep. | 35.0 $\mu$ W | 1.35 mW      | —      | 0.20 ms  | 0.28 $\mu$ J |
| Readout            | 48.0 $\mu$ W | 1.35 mW      | —      | 3.0 ms   | 4.2 $\mu$ J  |
| Total              |              |              |        |          | 120 mJ       |

TABLE II. Power and energy costs of “one-time” operations that contribute to the baseline energy expenditure. MW: Microwave.

more, the coherence time is prolonged by about two orders of magnitude, mainly due to the use of magnetic field shielding. Although faster gates imply higher energy consumption (for a given geometry), the energy consumption decreases when using fewer DD pulses, or completely omitting them. We expect a Toffoli gate to require 4 pJ and a gate time of 125  $\mu$ s, which eliminates the need for DD. Implementing the CNOT gate still requires two  $\pi/2$  pulses on the target qubit as well as two  $\pi$ -pulses on the target and control to decouple them from qubit 2, resulting in  $5\pi$ -pulses. In total, 20 nJ are required for the Half-Adder. This is approximately  $10^5$  times more efficient than the current setup (Table I), due to  $1000\times$  more efficient pulses and  $100\times$  fewer DD pulses. And still, this trap was not built with the specific goal of energy efficiency.

In the future, it is possible that radically different ion traps may increase the energy efficiency further. The radiation area ( $A_{\text{rad}}$ ) could be decreased to the order of magnitude of the ions’ effective dipole area ( $A_{\text{dip}}$ ) by using a cavity QED setup [42].

Efficient control protocols will become necessary in the “one-photon limit” [43]. To the best of our knowledge, this is still an open problem [44, 45]. Nevertheless, Stevens *et al.* [46] have recently observed that, indeed, typically one quanta of energy is used from control fields. Other strategies to reduce energetic costs may be reusing control energy, manipulating several qubits at once and/or recycling unused energy.

The energy efficiency of conventional processors is decelerating. Our work presents a path towards energy efficiency beyond CMOS, and offers a reversible platform to which future ones can be compared. We believe our detailed measurements of the cost of quantum operations will also be useful for groups interested in the energetics of quantum computation.

*Acknowledgements.*— SP and YO thank the support from FCT, namely through projects UIDB/50008/2020 and UIDB/04540/2020. SP thanks the support from the “la Caixa” foundation through scholarship No. LCF/BQ/DR20/11790030. PHH, PB, and CW acknowledge financial support from the EU Horizon 2020 project 820314 (microQC). Sagar Pratapsi and Patrick H. Huber contributed

equally to this work.

- 
- [1] Masanet, E., Shehabi, A., Lei, N., Smith, S. & Koomey, J. Recalibrating global data center energy-use estimates. *Science* **367**, 984–986 (2020).
- [2] Naffziger, S. & Koomey, J. Energy efficiency of computing: What’s next? *Electronic Design* (2016).
- [3] Landauer, R. Irreversibility and heat generation in the computing process. *IBM journal of research and development* **5**, 183–191 (1961).
- [4] Rabaey, J. M. & Pedram, M. (eds.) *Low Power Design Methodologies* (Springer US, Boston, MA, 1996). URL <http://link.springer.com/10.1007/978-1-4615-2307-9>.
- [5] Koomey, J. G. A primer on the energy efficiency of computing. In *AIP Conference Proceedings*, vol. 1652, 82–89 (American Institute of Physics, 2015).
- [6] Ni, J. & Bai, X. A review of air conditioning energy performance in data centers. *Renewable and Sustainable Energy Reviews* **67**, 625–640 (2017). URL <https://www.sciencedirect.com/science/article/pii/S136403211630541X>.
- [7] Fredkin, E. F. & Toffoli, T. *Design Principles for Achieving High-Performance Submicron Digital Technologies*, 27–46 (Springer-Verlag, Berlin, Heidelberg, 2001).
- [8] Fredkin, E. & Toffoli, T. Conservative logic. *International Journal of theoretical physics* **21**, 219–253 (1982). URL <https://doi.org/10.1007/BF01857727>.
- [9] Seitz, C. L. *et al.* Hot clock nmos. *Computer Science Technical Reports* (1985). URL <https://resolver.caltech.edu/CaltechCSTR:1985.5177-tr-85>.
- [10] Koller, J. & Athas, W. Adiabatic switching, low energy computing, and the physics of storing and erasing information. In *Workshop on Physics and Computation*, 267–270 (1992).
- [11] Hall, J. An electroid switching model for reversible computer architectures. In *Workshop on Physics and Computation*, 237–247 (1992).
- [12] Merkle, R. Towards practical reversible logic. In *Workshop on Physics and Computation*, 227–228 (1992).
- [13] Merkle, R. C. Reversible electronic logic using switches. *Nanotechnology* **4**, 21–40 (1993). URL <https://doi.org/10.1088/0957-4484/4/1/002>.
- [14] Drexler, K. E. *Molecular Machinery and Manufacturing with Applications to Computation*. Ph.D. thesis, Massachusetts Institute of Technology, USA (1992).
- [15] Drexler, K. E. *Nanosystems: Molecular Machinery, Manufacturing, and Computation* (John Wiley & Sons, Inc., USA, 1992).
- [16] Merkle, R. C. *et al.* Molecular mechanical computing systems. *Institute for Molecular Manufacturing, Palo Alto, CA, IMM Report* (2016).
- [17] Merkle, R. *et al.* Mechanical computing systems using only links and rotary joints. *Journal of Mechanisms and Robotics* **10** (2018).
- [18] Hogg, T., Moses, M. S. & Allis, D. G. Evaluating the friction of rotary joints in molecular machines. *Mol. Syst. Des. Eng.* **2**, 235–252 (2017). URL <http://dx.doi.org/10.1039/C7ME00021A>.
- [19] Likharev, K. Dynamics of some single flux quantum devices: I. parametric qantron. *IEEE Transactions on Magnetics* **13**, 242–244 (1977).
- [20] Hosoya, M. *et al.* Quantum flux parametron: a single quantum flux device for josephson supercomputer. *IEEE Transactions on Applied Superconductivity* **1**, 77–89 (1991).
- [21] Ren, J. & Semenov, V. K. Progress with physically and logically reversible superconducting digital circuits. *IEEE Transactions on Applied Superconductivity* **21**, 780–786 (2011).
- [22] Lent, C., Tougaw, P. & Porod, W. Quantum cellular automata: the physics of computing with arrays of quantum dot molecules. In *Proceedings Workshop on Physics and Computation. PhysComp '94*, 5–13 (1994).
- [23] Frank, M. P. Back to the future: The case for reversible computing. *arXiv preprint arXiv:1803.02789* (2018).
- [24] Benioff, P. The computer as a physical system: A microscopic quantum mechanical hamiltonian model of computers as represented by turing machines. *Journal of Statistical Physics* **22**, 563–591 (1980). URL <https://doi.org/10.1007/BF01011339>.
- [25] Benioff, P. Quantum mechanical models of turing machines that dissipate no energy. *Phys. Rev. Lett.* **48**, 1581–1585 (1982). URL <https://link.aps.org/doi/10.1103/PhysRevLett.48.1581>.
- [26] Moutinho, J. P. *et al.* Quantum dynamics for energetic advantage in a charge-based classical full-adder. *arXiv preprint arXiv:2206.14241* (2022).
- [27] Mano, M. M. & Kime, C. R. *Logic and computer design fundamentals* (Prentice-Hall, Inc., 1997).
- [28] Jaschke, D. & Montangero, S. Is quantum computing green? an estimate for an energy-efficiency quantum advantage. *arXiv* (2022). URL <https://arxiv.org/abs/2205.12092>.
- [29] Auffèves, A. Quantum technologies need a quantum energy initiative. *PRX Quantum* **3**, 020101 (2022). URL <https://link.aps.org/doi/10.1103/PRXQuantum.3.020101>.
- [30] Antonio, B., Randall, J., Hensinger, W. K., Morley, G. W. & Bose, S. Classical Computation by Quantum Bits. *arXiv:1509.03420 [quant-ph]* (2015). URL <http://arxiv.org/abs/1509.03420>. ArXiv: 1509.03420.
- [31] Wunderlich, C. *Conditional Spin Resonance with Trapped Ions*, 261–273 (Springer Berlin Heidelberg, Berlin, Heidelberg, 2002).
- [32] Khromova, A. *et al.* Designer spin pseudomolecule implemented with trapped ions in a magnetic gradient. *Phys. Rev. Lett.* **108**, 220502 (2012). URL <https://link.aps.org/doi/10.1103/PhysRevLett.108.220502>.
- [33] Piltz, C., Sriarunothai, T., Varón, A. & Wunderlich, C. A trapped-ion-based quantum byte with 10e-5 next-neighbour cross-talk. *Nat. Commun.* **5**, 4679 (2014).
- [34] Piltz, C., Scharfenberger, B., Khromova, A., Varón, A. F. & Wunderlich, C. Protecting conditional quantum gates by robust dynamical decoupling. *Phys. Rev. Lett.* **110**, 200501 (2013). URL <https://link.aps.org/doi/10.1103/PhysRevLett.110.200501>.
- [35] Maudsley, A. A. Modified carr-purcell-meiboomgill sequence for nmr fourier imaging applications. *Journal of Magnetic Resonance (1969)* **69**, 488–491 (1986). URL <https://www.sciencedirect.com/science/article/pii/0022236486901605>.
- [36] Genov, G. T., Schraft, D., Vitanov, N. V. & Halfmann, T. Arbitrarily accurate pulse sequences for robust dynamical decoupling. *Phys. Rev. Lett.* **118**, 133202 (2017). URL <https://link.aps.org/doi/10.1103/PhysRevLett.118.133202>.
- [37] Khromova, A. *Quantum gates with trapped ions us-*

ing magnetic gradient induced coupling. Ph.D. thesis, University of Siegen (2012).

- [38] Kiktenko, E. O., Norkin, D. O. & Fedorov, A. K. Confidence polytopes for quantum process tomography. *New Journal of Physics* **23**, 123022 (2021). URL <https://doi.org/10.1088/1367-2630/ac3cf7>.
- [39] Ježek, M., Fiurášek, J. & Hradil, Z. c. v. Quantum inference of states and processes. *Phys. Rev. A* **68**, 012305 (2003). URL <https://link.aps.org/doi/10.1103/PhysRevA.68.012305>.
- [40] Okhrimenko, B., Esteki, E., Boldin, I. & Wunderlich, C. In preparation (2022).
- [41] Allcock, D. T. C. *et al.* A microfabricated ion trap with integrated microwave circuitry. *Applied Physics Letters* **102**, 044103 (2013). URL <https://doi.org/10.1063/1.4774299>. <https://doi.org/10.1063/1.4774299>.
- [42] Sterk, J. D., Luo, L., Manning, T. A., Maunz, P. & Monroe, C. Photon collection from a trapped ion-cavity system. *Physical Review A* **85**, 062308 (2012). URL <https://link.aps.org/doi/10.1103/PhysRevA.85.062308>.
- [43] Gea-Banacloche, J. Minimum energy requirements for quantum computation. *Phys. Rev. Lett.* **89**, 217901 (2002). URL <https://link.aps.org/doi/10.1103/PhysRevLett.89.217901>.
- [44] Itano, W. M. Comment on “some implications of the quantum nature of laser fields for quantum computations”. *Phys. Rev. A* **68**, 046301 (2003). URL <https://link.aps.org/doi/10.1103/PhysRevA.68.046301>.
- [45] Gea-Banacloche, J. & Miller, M. Quantum logic with quantized control fields beyond the  $1/\bar{n}$  limit: Mathematically possible, physically unlikely. *Phys. Rev. A* **78**, 032331 (2008). URL <https://link.aps.org/doi/10.1103/PhysRevA.78.032331>.
- [46] Stevens, J. *et al.* Energetics of a single qubit gate. *Phys. Rev. Lett.* **129**, 110601 (2022). URL <https://link.aps.org/doi/10.1103/PhysRevLett.129.110601>.

## Supplemental material

### Choosing $\Omega$ coupling and gate time for the Toffoli evolution

We simulated the Hamiltonian evolution of Equation (1) numerically, for different values of  $\Omega$  and a total evolution time of  $\pi/\Omega$ . Given our limited coherence time, we focused on finding the fastest possible Toffoli gate.

We calculated the classical fidelity of each gate as the probability of obtaining the correct classical output state when given a uniformly random input computational state, when compared to a Toffoli gate. Our findings are summarised in FIG. 3.

We chose the fastest possible gate time, with  $\approx 14.9$  ms, corresponding to the right-most peak in FIG. 3. It is possible to find gate times with better fidelities. Although we are currently limited by coherence time, stronger  $J$  couplings might allow the other peaks of FIG. 3 to be experimentally realisable in the future.

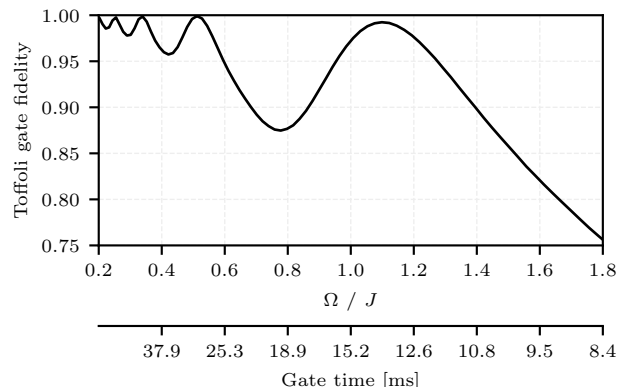


FIG. 3. **Classical Toffoli gate fidelity** as a function of the  $\Omega$  coupling’s strength in Eq. (3), measured in units of  $J = J_{12} = J_{23}$ . We simulated the Hamiltonian for a time of  $\pi/\Omega$  (bottom axis). The right-most peak, with  $\Omega = 1.1J$ , allows for a 14.9 ms gate with approximately 99% fidelity.

### Theoretical energy estimate

The Rabi frequency  $\Omega_R$  of a magnetic dipolar transition, like that between the two states  $|0\rangle$  and  $|1\rangle$ , is a function of the magnetic field surrounding the ion,

$$\hbar\Omega_R = \boldsymbol{\mu} \cdot \mathbf{B}_{\text{amp}}, \quad (5)$$

where  $\mathbf{B}_{\text{amp}}$  is the magnetic field amplitude and  $\boldsymbol{\mu} = \langle 1|\mathbf{M}|0\rangle$  is the magnetic dipole moment of the transition. The Rabi frequency  $\Omega_R$  is experimentally accessible. We estimate  $\mu = \mu_B$ , where  $\mu_B$  is the Bohr magneton. Having these two quantities, we can estimate the value of  $\mathbf{B}_{\text{amp}}$  which, in turn, will allow us to calculate the energy carried by the electromagnetic field of the microwave pulse. To do so, we need to know the profile of the microwave field’s wave front.

To generate the microwave field, we use an OFHC copper cylindrical cavity resonator of diameter  $2a \approx 16.3$  mm, placed inside the vacuum chamber [37]. The dimensions of the cavity were chosen specifically to allow the propagation of the dominant transverse-electric mode,  $\text{TE}_{11}$ , at the qubit frequency 12.6 GHz, while suppressing higher-order modes.

To estimate the energy carried by the microwave's field, we assume that the ions are placed near the open end of the microwave cavity, close to its cylindrical axis, and that the magnetic field at that point may be approximated by the  $\text{TE}_{11}$  mode of an infinite circular wave guide of the same diameter. Let us use a cylindrical coordinate system  $\rho, \phi, z$ , where  $z$  is aligned with the cylinder axis. Let us calculate the intensity of the fields of the  $\text{TE}_{11}$  mode by assuming a time and  $z$  dependence like

$$\mathbf{E}, \mathbf{B} \propto e^{i(\omega t - \beta z)}. \quad (6)$$

From Maxwell's equations for the vacuum inside the waveguide we can obtain expressions for the EM fields as a function of the  $E_z$  and  $B_z$  components

$$\begin{aligned} \begin{bmatrix} E_\rho \\ B_\phi \end{bmatrix} &= \frac{-i}{k_c^2} \begin{bmatrix} \beta & \omega \\ k/c & \beta \end{bmatrix} \begin{bmatrix} \partial_\rho E_z \\ \partial_\phi B_z / \rho \end{bmatrix} \\ \begin{bmatrix} B_\rho \\ E_\phi \end{bmatrix} &= \frac{-i}{k_c^2} \begin{bmatrix} \beta & -k/c \\ -\omega & \beta \end{bmatrix} \begin{bmatrix} \partial_\rho B_z \\ \partial_\phi E_z / \rho \end{bmatrix}, \end{aligned} \quad (7)$$

where  $k_c^2 = k^2 - \beta^2$  and  $k = \omega/c$ .

The resonator was designed to allow only transverse electric fields, that is,  $E_z = 0$ . Applying  $\nabla \cdot \mathbf{B} = 0$ , and assuming a separation of variables  $B_z = B_0 R(\rho) \Phi(\phi)$ , we arrive at

$$\partial_\phi^2 \Phi + \alpha^2 = 0 \quad (8)$$

$$(\rho \partial_\rho)^2 R + (\rho^2 k_c^2 - \alpha^2) R = 0, \quad (9)$$

for some constant  $\alpha$ .

Equation (8) has the general solution  $\Phi(\phi) = A \cos(\alpha(\phi - \phi_0))$ . Imposing  $\Phi(\phi + 2\pi) = \Phi(\phi)$  restricts  $\alpha$  to integer values. Equation (9) is the *Bessel functional equation*. The only solutions that do not diverge are the Bessel functions of the first kind,  $J_\alpha(k_c \rho)$ . Since  $J_{-\alpha}$  and  $J_\alpha$  are equal up to a  $\pm 1$  factor, we will take  $\alpha$  to be a non-negative integer and rename it to  $\alpha = n \in \mathbb{N}$ . We thus arrive at the solution

$$B_z = B_0 J_n(k_c \rho) \cos(n(\phi - \phi_0)) e^{i(\omega t - \beta z)}. \quad (10)$$

The remaining field components can be calculated from Equations (7),

$$\begin{aligned} E_\rho &= \frac{i\omega B_0 n}{k_c} \frac{J_n(k_c \rho)}{k_c \rho} \sin(n(\phi - \phi_0)) e^{i(\omega t - \beta z)} \\ E_\phi &= \frac{i\omega B_0}{k_c} J'_n(k_c \rho) \cos(n(\phi - \phi_0)) e^{i(\omega t - \beta z)} \\ B_\rho &= -\frac{i\beta B_0}{k_c} J'_n(k_c \rho) \cos(n(\phi - \phi_0)) e^{i(\omega t - \beta z)} \\ B_\phi &= \frac{i\beta B_0 n}{k_c} \frac{J_n(k_c \rho)}{k_c \rho} \sin(n(\phi - \phi_0)) e^{i(\omega t - \beta z)}, \end{aligned}$$

where  $J'_n$  is the derivative of the  $n$ -th Bessel function.

Finally, there is the added restriction that  $\mathbf{E}$  be perpendicular to the conductor's surface, that is,  $E_\phi(\rho = a) = 0$ , which means that

$$k_c a = p'_{nm}, \quad (11)$$

where  $p'_{nm}$  is the  $m$ -th root of  $J'_n$ . For each  $n, m$  there is a different solution – the so-called  $\text{TE}_{nm}$  modes.

We will now focus on the  $\text{TE}_{11}$  mode, for  $n = 1$ , which is the first non-zero solution to Equations (8) and (9), also called the *dominant mode*, and also the only allowed mode of propagation by our cavity. In this case, we have  $k_c a = p'_{11} \approx 1.8412$ .

To calculate the energy carried by the microwave pulse, we calculate the Poynting vector and average it over a period  $T = 2\pi/\omega$ ,

$$\mathbf{S}^{\text{avg}} = \frac{1}{T} \int_0^T \frac{\mathbf{E} \times \mathbf{B}}{\mu_0} dt. \quad (12)$$

The only non-zero component of this vector is in the  $z$  direction,

$$\begin{aligned} S_z^{\text{avg}} &= \frac{1}{2} \frac{B_0^2}{\mu_0} \frac{\omega \beta}{k_c^2} \left[ \left( \frac{J_1(k_c \rho)}{k_c \rho} \sin(\omega t - \beta z) \right)^2 \right. \\ &\quad \left. + \left( J'_1(k_c \rho) \cos(\omega t - \beta z) \right)^2 \right]. \end{aligned} \quad (13)$$

We now integrate over the entire cross-section of the cylinder to obtain the power delivered by the cavity,

$$P = \frac{1}{2} \frac{B_0^2}{\mu_0} \frac{\omega \beta}{k_c^2} \frac{I_{11}}{(p'_{11})^2} \pi a^2, \quad (14)$$

where  $I_{11}$  is an integral of Bessel functions,

$$I_{11} = \int_0^{p'_{11}} \left[ \left( \frac{J_1(r)}{r} \right)^2 + \left( J'_1(r) \right)^2 \right] r dr \approx 0.405. \quad (15)$$

Finally, to estimate the power, we need only find the value of  $B_0$  that makes the qubit states flop at the observed Rabi frequency  $\Omega_R$ . The magnetic field amplitude at the center of the waveguide is

$$B_{\text{amp}} = \|\mathbf{B}(\rho = 0)\|_{\text{max}} = \frac{\beta}{k_c} \frac{B_0}{2} = \frac{\hbar \Omega_R}{\mu \cos \theta}. \quad (16)$$

The last equality comes from Equation (5). The angle  $\theta$  is that between the ions' magnetic dipole moment and the cavity's magnetic field.

We then arrive at the expression for the power carried by the microwave pulse,

$$P = \frac{1}{2} \frac{A_{\text{rad}}}{A_{\text{dip}}} \frac{\hbar \Omega_R^2}{\cos^2 \theta}, \quad (17)$$

where we defined the areas

$$A_{\text{rad}} = \frac{4I_{11}}{(p'_{11})^2} \frac{\pi a^2}{\sqrt{1-x^2}} \quad \text{and} \quad A_{\text{dip}} = \frac{\mu_0}{\hbar c} \mu^2, \quad (18)$$

with  $x = cp'_{11}/\omega a$ . The area  $A_{\text{dip}}$  can be thought of as an effective dipole cross-section for the ion.